Article

Structure-Property Relationships of Polyethylene Glycol Modified Fluorophore as Near-infrared A# Imaging Probes

Kaixiang Zhou, Yuying Li, Yi Peng, Xiaomei Cui, Jiapei Dai, and Mengchao Cui

Anal. Chem., **Just Accepted Manuscript** • DOI: 10.1021/acs.analchem.8b01712 • Publication Date (Web): 14 Jun 2018

Structure-Property Relationships of Polyethylene Glycol Modified Fluorophore as Near-infrared Aβ Imaging Probes

Kaixiang Zhou[a], Yuying Li[a], Yi Peng[a], Xiaomei Cui[a, b], Jiapei Dai[c], Mengchao Cui[a,*]

[a] Key Laboratory of Radiopharmaceuticals, Ministry of Education, College of Chemistry, Beijing Normal University, Beijing 100875, China

[b] Department of Chemistry and Environmental Sciences, Tibet University, Lhasa 850000, China

[c] Wuhan Institute for Neuroscience and Neuroengineering, South-Central University for Nationalities, Wuhan 430074, China

ABSTRACT: To optimize the lipophilicity and improve *in vivo* pharmacokinetics of near-infrared probes targeted Aβ plaques, we designed, synthesized and evaluated a series of polyethylene glycol modified probes with hydroxyl and methoxyl terminals. The relationships between chemical structure and optical, biological properties were systemically elucidated. The results indicated that a desired Aβ probe should keep a balance among molecular rigidity, size, and lipophilicity. Probe **12d** displayed improved properties including intense and selective response to A$\beta_{1\text{-}42}$ aggregates (K_d = 7.3 nM, 22 fold fluorescence enhancement and emission maxima at 715 nm upon interaction with A$\beta_{1\text{-}42}$ aggregates), sufficient blood-brain barrier penetration (3.04 % ID/g), and fast wash out from the brain ($brain_{2min}/brain_{60min}$ = 10.1). Clear fluorescence signals retention in transgenic mice than control mice in *in vivo* near-infrared imaging. Hence, polyethylene glycol modified probes retained favorable optical properties but displayed great improvement of biological properties for Aβ detection.

INTRODUCTION

Alzheimer's disease (AD) is a neurodegenerative disorder that severely influences millions of people with the exacerbation of the population ages, while there is no cure or stoppable therapies yet available[1]. To date, there's still debate about the nosogenesis of AD, the well-established amyloid cascade hypothesis points out that the accumulation and deposition of the β-amyloid (Aβ) plaques is responsible for this disease. The proteolysis pathway of the amyloid precursor protein produced Aβ_{40} and Aβ_{42} fragments by β- and γ-secretases, and these Aβ monomers are easily aggregated to oligomers, fibers and finally piled into Aβ plaques. The excess accumulation of Aβ plaques lead to reduction of neurotransmitters, cognition defects and synaptic plasticity[2-4]. More recently, Moir and coworkers revealed Aβ protein could act as antimicrobial peptides and exert positive physiological functions. The increased Aβ generation may be the response of the received infection or sterile inflammatory stimuli. Hence, Aβ protein plays a protective role in innate immunity in the brain[5, 6]. In any case, the aggregated Aβ protein is still believed to have close connection with AD, trace or monitor the level of Aβ aggregates in the brain may provide ample and embedded information to better understand AD. In recent years, much effort have been devoted to detect Aβ plaques non-invasively in the early stage of AD, and various imaging techniques such as single-photon emission-computed tomography (SPECT)[7], positron emission computed tomography (PET)[8] and optical imaging[9] were employed.

PET and SPECT are powerful imaging tools and widely used all over the world, however, their tracers must be labeled with proper radionuclides, high cost, and exposure to the radioactivity impeded their extensive application. As an alternative to radionuclide imaging, fluorescence-based optical imaging gained incremental interest for detection of physiological and biochemical process both *in vitro* and *in vivo*. However, fluorescence imaging is limited due to the poor light penetration of the biological tissues, but it's uplifting to remark that the light in the near-infrared (NIR) region (650 - 900 nm) have better tissue penetration and make it possible to real-time imaging in living organism[10-14]. With the assistant of NIR light, it's possible to achieve depth imaging, decrease the photodamage and avoid autoflourescence from biological matters[9]. NIR optical imaging using probes targeting to Aβ aggregates in the brain is a strategy used to detect AD non-invasively *in vivo*. A number of small NIR probes including charged oxazine dyes[15] and styryl-based cyanine dyes[16], as well as neutral probes such as bithiophene derivatives[17], difluoroboronate curcumin derivatives[18-20], thiophene derivatives[21], styrylpyran derivatives[22-24], and boron-dipyrromethene probes[25] were developed to label or monitor Aβ species in the brain. These probes were commonly designed on the basis of pull-push structure with electron donor and acceptor bridged by conjugated π system (D-π-A). Since 2014, according to the D-π-A structure, our group reported series of smart Aβ probes with different kinds of electron acceptors, such as malononitrile, methyl cyanoacetate, dimethyl malonate, meldrum's acid, dimedone, and barbituric acid[26, 27], among these probes, 2-((2E,4E)-5-(4-(dimethylamino)phen yl)penta-2,4-dien-1-ylidene)malononitrile (DANIR 2c)[28] exhibited excellent ability to image Aβ plaques in living mouse. Thereafter, (E)-2-(3-(6-(dimethylamino)naphthalen-2-yl)allyli dene)malononitrile (DANIR 3b)[29] and 2-((2E,4E)-5-(6-((2-hydroxyethyl)(methyl)amino)naphthalen-2-yl)penta-2,4-dien-1-ylidene)malononitrile (DANIR 8c)[30] with a naphthalene π bridge were reported, compared with DANIR 2c, they dis-

played high quantum yield and more favorable *in vivo* properties. More recently, we expanded the scope of these D-π-A probes and systemically elucidated the relationships between π-conjugated system (different lengths of polyenic chains and aromatic rings) and properties (optical and biological)[31]. Polyethylene glycol (PEG) chains are connected by repeated units of ethylene glycol monomer and demonstrated favorable function on pharmacokinetic and pharmacodynamic in polypeptide drugs[32]. Since 2005, Zhang et al. reported the conjugation of short PEG chains to Aβ homing ligands with a terminal fluorine-18 atom, and achieved simple adjustment of the ligand lipophilicity and better *in vivo* pharmacokinetics[33, 34]. In this study, to further investigate the relationship between structure and properties including optical and biological, we applied short PEG chains with hydroxyl and methoxyl terminals to the electron acceptors of naphthalene ring based D-π-A probes.

EXPERIMENTAL SECTION

General Information. Reagents and solvents were analytical-grade and were purchased from OuheChem, TCI, and J&K Chemicals and used without further purification. Reactions were monitored by thin layer chromatography (TLC) plates (aluminum sheets with silica gel 60 F_{254} plates, Merck). Column chromatography was carried out with silica gel (45 - 75 μm, Yantai Industry Research Institute). Synthetic A$\beta_{1\text{-}42}$ peptides were purchased from Peptide Institute, Inc. (Japan), and A$\beta_{1\text{-}42}$ fibers for *in vitro* assays were aggregated using the procedures reported previously[35]. ^{1}H and ^{13}C NMR spectra were recorded on a Bruker Avance III (400 MHz or 100 MHz, Germany) spectrometer in $CDCl_3$, CF_3COOD or DMSO-d_6 solutions at room temperature (rt). Chemical shift (δ) is reported in ppm downfield from tetramethylsilane (TMS) and coupling constants (J) are reported in Hertz (Hz), and the multiplicity is defined by s (singlet), d (doublet), t (triplet) or m (multiplet). Mass spectrometry (MS) were acquired by the Surveyor MSQ Plus (ESI) (Waltham, MA, USA) instrument. High resolution mass spectra (HRMS) were acquired by Thermo scientific Q-Exactive (ESI) (USA) mass spectrometer. Fluorescence spectra were measured on a RF-5301PC spectrofluorophotometer (Shimadzu, Japan). The absolute fluorescence quantum yields were acquired by the Absolute PL Quantum Yield Spectrometer C11347 (Hamamatsu, Japan). UV-visible spectra were carried out on the UV-3600 UV-Vis spectrophotometer (Shimadzu, Japan). High-performance liquid chromatography (HPLC) was conducted on Primaide system (Hitachi, Japan). The sample was analyzed on a Venusil MP C18 reverse column (5 μm, 4.6 mm×250 mm, Bonna-Agela Technologies, China) eluted with an isocratic system at a flow rate of 1.0 mL/min, mobile phase was water and acetonitrile, respectively. Fluorescence observation was performed on EVOS FL imaging system equipped with GFP, RFP, Texas Red, and CY5 filter sets (Life, USA). UV absorbance was read at 490 nm on Epoch microplate spectrophotometer (Biotek, USA). Male ICR mice (4 weeks, 18 - 22 g) used for brain uptake studies were purchased from Beijing Vital River Laboratories (China). Double transgenic mice (C57BL6, APPsw/PSEN1, 19-month old) used as AD model and age-matched control mice (C57BL6, 19-month old) were purchased from Institute of Laboratory Animal Sciences, Chinese Academy of Medical Sciences. Postmortem brain tissues of temporal lobe from autopsy confirmed AD patients (91-year old, male; 68-year old, female; 64-year old, female; 76-year old, male; 71-year-old, female; 85-year-old, male) and healthy humans (68-year old, female; 80-year old, female; 84-year old, male; 89-year old, male; 74-year old, male) were obtained from Chinese Brain Bank Center. All protocols requiring the use of animals were approved by the animal care committee of Beijing Normal University.

Chemistry. The PEG modified acceptors (**1 - 6**) and the final NIR probes were outlined in Scheme 1 and S1 in Supporting Information. Details of synthesis, original ^{1}H NMR, ^{13}C NMR, MS, and HRMS spectra were also included in Supporting Information.

Spectroscopic Determination. Ultraviolet absorption spectra, fluorescence spectra and absolute quantum yields of these probes in various solvents were tested using traditional methods. The fluorescence interaction of selected probes with A$\beta_{1\text{-}42}$ aggregates and bovine serum albumin (BSA) were determined according to our reported methods[26, 28].

Biological Evaluations. *In vitro* fluorescence staining on brain sections, *in vitro* saturation binding assay using A$\beta_{1\text{-}42}$ aggregates, *in vitro* stability study, cytotoxicity study, brain entry values and kinetics in normal mice, *in vivo* NIR imaging and *ex vivo* histopathological staining in transgenic and age-matched control mice were completed using our reported methods[26, 28], the detailed procedures were described in Supporting Information.

RESULTS AND DISCUSSION

NIR Probes Synthesis

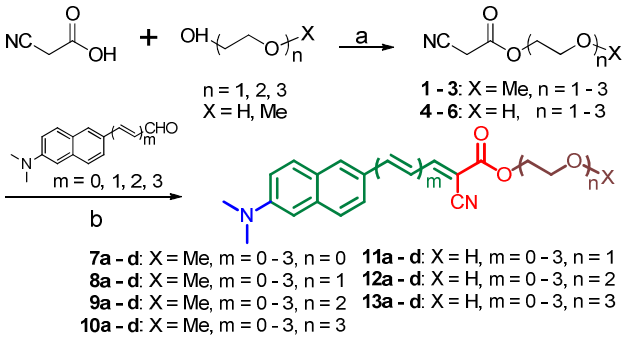

Scheme 1. Reagents and conditions: (a) DCC, DMAP, anhydrous CH_2Cl_2, rt, 5 h; (b) piperidine, MeOH or CH_2Cl_2, 60 °C, reflux, 3 h.

Chemical synthesis was applied according to the methods shown in Scheme 1. Naphthyl aldehydes with different lengths of polyenic chains were obtained by iterative Wittig reaction following the similar methods reported previously[31]. The PEG modified acceptors (**1 - 6**) were produced by esterification from 2-cyanoacetate acid and short PEG chains (n = 1 - 3) with hydroxyl and methoxyl terminals, dicyclohexylcarbodiimide (DCC) and 4-dimethylaminopyridine (DMAP) were employed as dehydrant and catalyst, respectively. The final NIR probes (**7a-c** to **13a-c**) were readily synthesized using Knoevengel condensation between appropriate naphthyl aldehydes and PEG modified cyanoacetate substrates catalyzed by small amount of piperdine. All the probes were verified by ^{1}H, ^{13}C NMR, HRMS and proved to be greater than 95% purity with HPLC. It should be noted that unlike our previously reported Knoevengel condensations using methanol or ethanol as solvents, for these PEG modified cyanoacetate substrates, transesterification is much more likely to happen in methanol

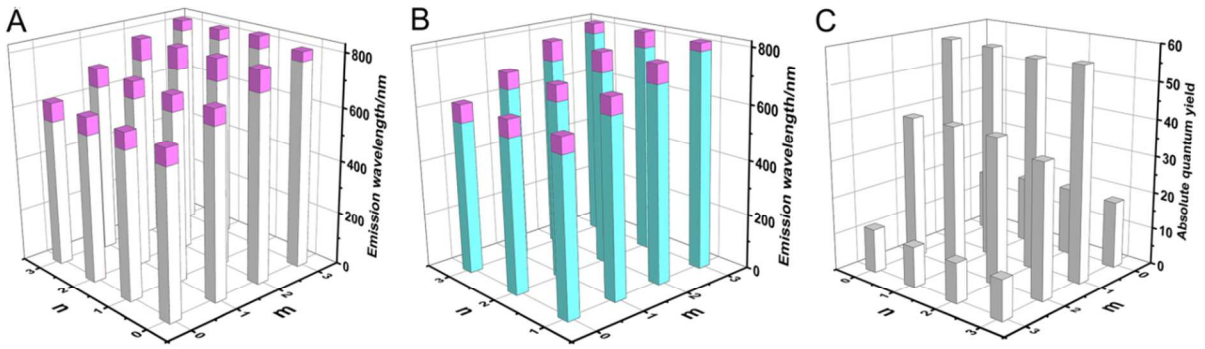

Figure 1. Fluorescent properties associated with the length of conjugated double bond and PEG chain. (A) Maximum emission of methoxyl-ended probes (**8a-d** to **10a-d**) measured in CH_2Cl_2 (white) and PBS (magenta). (B) Maximum emission of hydroxyl-ended probes (**11a-d** to **13a-d**) measured in CH_2Cl_2 (cyan) and PBS (magenta). (C) Absolute quantum yield of methoxyl-ended probes (**7a-d** to **10a-d**) determined in CH_2Cl_2.

Table 1. Selected spectroscopic and biological data for the synthesized probes.

Probe	λ_{em1} [a]	λ_{ex1} [a]	λ_{em2} [b]	Φ/%	Fold [e]	K_d (nM) [f]	Brain Entry (% ID g^{-1}) [g]
7a	618	472	n.d.	16.6 [c]/0.8 [d]	n.d.	359.13 ± 77.21	n.d.
7b	700	493	615	58.2/0.7	216.7	39.44 ± 12.32	n.d.
7c	788	619	660	39.2/0.2	122.1	10.34 ± 1.05	2.98 ± 0.43
7d	801	630	700	11.8/0.1	31.0	8.11 ± 0.65	1.42 ± 0.46
8a	620	471	n.d.	18.1/0.9	n.d.	164.5 ± 10.22	0.00 ± 0.00
8b	700	493	610	57.9/1.0	220.4	30.92 ± 6.38	0.40 ± 0.09
8c	788	622	662	39.5/0.1	150.2	30.97 ± 5.37	1.75 ± 0.25
8d	830	635	710	10.9/0.1	33.8	23.1 ± 10.43	1.00 ± 0.23
9a	622	471	n.d.	18.5/0.9	n.d.	415.17 ± 93.57	n.d.
9b	705	501	613	56.8/1.2	186.1	39.99 ± 12.84	n.d.
9c	788	620	662	39.4/0.2	159.3	24.59 ± 4.89	2.69 ± 0.25
9d	800	624	712	10.8/0.1	20.2	15.37 ± 3.4	1.07 ± 0.19
10a	625	479	n.d.	78.2/0.9	n.d.	467.33 ± 136.5	n.d.
10b	710	500	615	57.3/1.3	180.5	32.93 ± 7.63	n.d.
10c	785	620	663	36.1/0.2	163.1	6.49 ± 1.06	1.74 ± 0.43
10d	820	636	718	29.4/0.2	10.8	15.93 ± 3.81	1.60 ± 0.59
11a	622	479	n.d.	19.4/0.8	n.d.	144.77 ± 4.25	0.85 ± 0.09
11b	708	500	614	52.1/1.0	161.0	46.49 ± 6.1	3.38 ± 0.26
11c	780	615	664	32.9/0.3	125.9	52.16 ± 9.6	3.87 ± 0.01
11d	817	636	720	9.8/0.1	27.4	8.24 ± 1.65	2.16 ± 0.15
12a	624	476	n.d.	17.8/0.9	n.d.	152.4 ± 1.31	n.d.
12b	700	494	618	53.6/1.1	118.0	62.43 ± 8.4	n.d.
12c	780	615	662	37.3/0.2	90.8	51.32 ± 11.29	3.18 ± 0.66
12d	820	639	715	11.0/0.1	21.8	7.28 ± 3.54	3.04 ± 0.84
13a	623	485	n.d.	17.8/0.9	n.d.	259.53 ± 50.63	n.d.
13b	700	500	620	53.1/1.2	99.0	49.16 ± 12.6	n.d.
13c	781	610	665	36.4/0.1	80.2	44.57 ± 10.81	3.17 ± 0.40
13d	817	641	720	10.5/0.1	23.5	35.03 ± 12.1	2.56 ± 0.53

[a]Emission/Excitation maxima determined in PBS. [b]Emission maxima upon binding to Aβ_{1-42} aggregates. Absolute quantum yield measured in CH_2Cl_2 [c] and PBS [d]. [e]Fluorescence enhancement upon binding to Aβ_{1-42} aggregates. [f]K_d values of NIR probes were measured in triplicate with results given as the mean ± SD. [g]Initial brain uptake after *i.v.* injection at 2 min, the values were shown as the mean ± SD (n = 3).

and only give the methyl cyanoacetate products. Thus for the synthesis of **8a-c** to **13a-c**, CH_2Cl_2 was selected as solvent.

Optical Properties

In this study, our probes are composed of dimethylamino donors, naphthalene and polyene based π bridge, and PEG modified cyanoacetate acceptors, which possess typical D-π-A architecture, and they could form an internal charge transfer (ICT) state. In general, ICT probes exhibited great solvatochromism due to the diverse stabilization of the dipole moment between ground and excited states in solvents with different polarity[9,36]. Hence, the solvatochromism is a good pathway to perform specific signal for the fluorescence probes upon responded target. As shown in Figure 1A, B, S1-7 and Table 1, S2-3, our probes displayed highly sensitive to solvent polarity (in five slovents), and give bathochromic shifts around 40 to 100 nm from tetrahydrofuran to phosphate buffer saline (PBS) (concentration of 0.01 M). The narrowed HOMO-LUMO gap contributed to the bathochromic shift of the absorption and emission wavelength, and extend the conjugated-π system is the most effective way to achieve a HOMO-LUMO gap reduction[37, 38]. As expected, for each additional trans double bond added to these probes, the λ_{em} increased about 80 nm in CH_2Cl_2, and finally we pushed the maxima emission wavelength to the NIR region, for probes with three or four conjugated double bonds, their λ_{em} were greater than 750 nm in PBS (0.01 M) solutions. In addition, these probes displayed high quantum yield (10% - 58%) in CH_2Cl_2 solution with a trend of rise first then decrease by expanding the conjugated-π system (Figure 1C), and this regular pattern is completely in accordance with our previous studies[31]. It is also found that the pegylated acceptors (n = 0 - 3, with hydroxyl and methoxyl terminals) has minor effect on optical properties. Compared with the probes with malononitrile acceptors[29], the probes with PEG modified cyanoacetate acceptors reach a same convergence of absorption maxima, emission maxima, Stokes shift and quantum yield. In general, these properties were mainly dominated by the conjugated system area, moreover, we could conclude that malononitrile and cyanoacetate has similar electron withdrawing ability, and we can improve their biological properties by simply modify the cyanoacetate acceptors without affecting optical properties.

The fluorescence switch on based biosensor provides a simple and quick analysis tool for the detection of specific proteins[12]. As shown in Table 1 and Fig S15-22, our probe achieved "turn on" phenomenon reposed on the sensitivity of D-π-A structure to the polarity of surrounding environmental, the quantum yield of probe in CH_2Cl_2 is greatly increased compared to PBS (0.01 M) with more polarity. This phenomenon could be corroborated by the results of intense fluorescence enhancement (20.2 - 220.4 fold) accompanied with significant hypsochromic shift (101 - 141 nm) of these probes when bound to Aβ_{1-42} aggregates. The "turn on" mechanism could be considered that our probes bind to the hydrophobic area of Aβ aggregates. Similar to our previous studies[31], signal enhancement was gradually reduced when increase the length of conjugated-π system while the length of PEG chain has little effect on this. The fluorescence enhancement of the hydroxyl-ended probes (**11a-d** to **13a-d)** was slight lower than methoxyl-ended probes (**7a-d** to **10a-d**), which means that the hydrogen bond formed by hydroxyl group may reduce the hydrophobic interaction between probes and Aβ aggregates. In addition, very weak interaction between our probes with bovine serum albumin and monomeric Aβ peptide (for **12d**) indicated low non-specific binding. In general, the hypsochromic shift of probes upon binding to Aβ aggregates usually bring negative effect，which may push the emission band out of NIR region, fortunately, the emission maxima of the NIR probes with three and four conjugated double bonds were in excess of 650 nm upon interaction with Aβ aggregates. These results suggested that our probes meet the fluorescent prerequisites as NIR sensor.

Histopathological Staining

In vitro fluorescence staining on formalin-fixed brain slices from transgenic (Tg) mice model (APPswe/PSEN1) of AD, autopsy-confirmed AD patients and patients with cerebral amyloid angiopathy (CAA) was selected as the easiest method to screen the binding ability of these NIR probes to Aβ plaques. As shown in Figure S23-26, all probes could specifically label Aβ deposits on brain tissues from Tg mice and AD patients. Taking probe **12d** as an example, we select brain tissues from four AD and two CAA patients to further validate it's binding ability to Aβ deposits. Various Aβ forms such as diffuse plaques (Fig 2C, D), dense-core plaques (Fig 2A, F) and vascular plaques (Fig 2B, E) could be stained by probe **12d**, which suggest that **12d** possessed hypersensitive to the β-sheet structure of Aβ deposits. Negative staining was observed on the brain slices from five healthy humans and a wild-type (WT) mouse, indicate low non-specific binding (Figure S27).

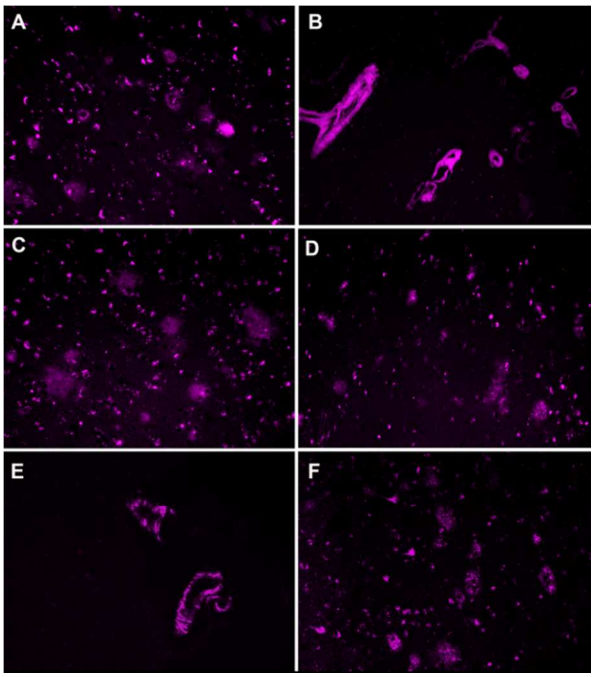

Figure 2. *In vitro* histopathological fluorescence staining of probe **12d** on brain slices from patients of AD and CAA. (A) AD tissue, 64-year old, female, temporal lobe, 20X; (B) CAA tissue, 68-year old, female, temporal lobe, 10X; (C) AD tissue, 71-year old, female, temporal lobe, 20X; (D) AD tissue, 85-year old, male, temporal lobe, 20X; (E) CAA tissue, 76-year old, male, temporal lobe, 20X; (F) AD tissue, 91-year old, male, temporal lobe, 20X.

Saturation Binding Assay

Thanks to the fluorescence enhancement effect of these probes upon binding to Aβ_{1-42} aggregates, we can measure quantitative binding affinity of these NIR probes to Aβ_{1-42} aggregates by saturation binding assays. As shown in Figure 3B, S28-31 and Table 1, they displayed enhancive binding affinity towards prolonged polyenic chains, while the length of PEG chains with hydroxyl or methoxyl terminals didn't express

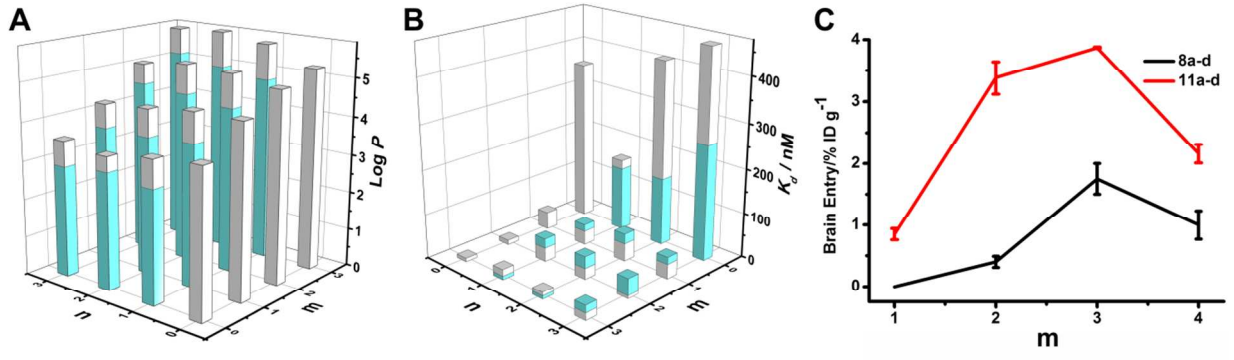

Figure 3. (A) The clog*P* value of the NIRF probes **7a - 10d** (methoxyl-ended probes) (white), **11a - 13d** (hydroxyl-ended probes) (cyan), calculated by the online ALOGPS 2.1 program. (B) K_d value for **7a - 10d** (white), **11a - 13d** (cyan). (C) Initial brain uptake of the **8a - 8d** (black curve) and **11a -11d** (red curve) after i.v. injection at 2 min.

regular or negative impact on binding affinity. In previous study, the malononitrile acceptor conjugated well to the π bridge to form a coplanar structure, which is favourable for A*β* binding. However, the probes with unconjugated PEG chains have more torsion may block their ready access to A*β* fibrils. Compared to the probes with malononitrile acceptor (DANIR 3a-c)[29], the binding affinity of PEG modified probes is slightly decreased, but still good enough to bind to A*β* aggregates. In summary, all these results indicate that conjugated π bridge is the essential factor in binding affinity and PEG modification is a straightforward method to adjust the hydrophilicity without passive effect on binding affinity.

Brain Penetration and Clearance Study

Optimal lipophilicity is one of the most important factors contributed to the blood-brain barrier (BBB) penetration ability of small molecule through passive diffusion[39,40]. As expected, lipophilicity of the probes (clog*P*) increases with the extend of conjugated π system, meanwhile, the increase of PEG chains has little effect on clog*P* value, mainly due to the relative short PEG units (n = 1 - 3). In addition, after adding hydroxyl group, the probe lipophilicity has reduced obviously (Figure 3A). Compared with DANIR 3a-c, methoxyl-ended probes (**7a-d** to **10a-d**) exhibited increased lipophilicity with the same length of polyenic chains, while hydroxyl-ended probes (**11a-d** to **13a-d**) decreased. Then the brain uptakes were measured by a HPLC based quantification method, concentrations of the probes in the brain homogenate were analyzed using HPLC after intravenous (*i.v.*) injection to ICR mice. As shown in Table 1, under the same length of polyenic chain, hydroxyl-ended probes (**11a-d** to **13a-d**) displayed higher initial brain uptake than methoxyl-ended probes (**7a-d** to **10a-d**), while the number of PEG units has less impact on the brain uptake. In order to study the effects of polyenic chain on brain uptake, we selected probe **8a-d** and **11a-d** with same PEG unit (n = 1) but different length of polyenic chain (m = 0 - 3). In accordance with our previous results, the initial brain uptake of these probes increase first and then decrease; by extending the number of polyenic unit (Figure 3C). However, compared with DANIR 3a - c, the PEG modified probes in this study displayed lower brain uptake, which indicate that molecular weight and size have negative effect on the ability of brain penetration. In addition, according to our previous studies, the brain kinetics of probes expressed as clearance rate decreased sharply with expanding polyenic chains probably due to the increase of lipophilicity, e.g. DANIR 3c with three conjugated double bonds displayed much lower clearance rate than DANIR 3b with two double bonds ($brain_{2min}/brain_{60min}$: 3.7 vs 21.7)[29]. However, the PEG modified probe **12d** with four conjugated double bonds still possess satisfactory wash-out rate ($brain_{2min}/brain_{60min}$ = 10.1), which verified the incorporate of PEG chains is benefit for pharmacokinetic. All these results demonstrated that lipophilicity of probe has strong relativity to their initial brain uptake and kinetics, the PEG modification is a simple way to adjust and improve these properties of NIR probes.

In addition, **12d** displayed high stability in PBS or in the presence of reducing agents including glutathione and cysteine (Figure S32). Furthermore, from the results of MTT assay, **12d** displayed poor cytotoxicity to human neuronal cell line (SH-SY5Y) (Figure S33).

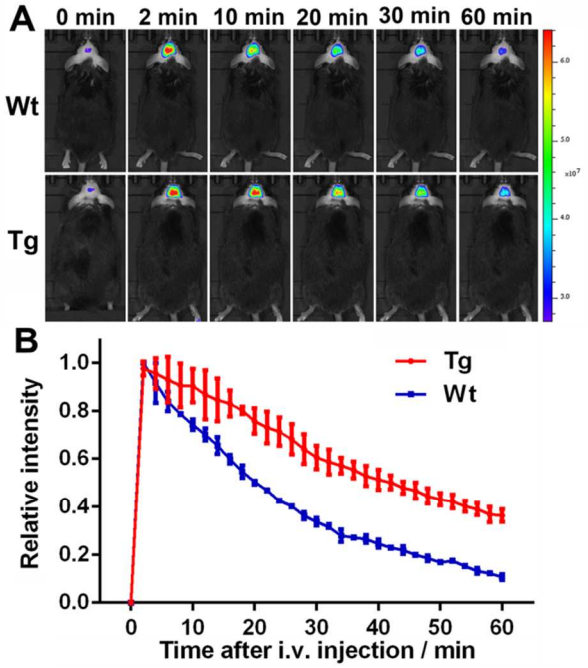

Figure 4. (A) *In vivo* NIR brain images from Tg and WT control mouse on representative time points before and after *i.v.* injection of probe **12d**. (B) Quantitative analysis of the relative fluorescence signals to show the brain kinetic curves of probe **12d** at selected time points.

***In vivo* NIR Imaging**

Finally, to investigate the *in vivo* imaging capacity of the NIR probes, probe **12d** with favorable optical and biological prop-

erties was selected for non-invasive detection of Aβ plaques in Tg mice (C57BL6, APPsw/PSEN1, 19-month old, male), and age-matched WT mice as control. After *i.v.* injection of **12d**, one hour dynamic imaging was acquired by an IVIS Lumina III system with time intervals of 2 minutes. Quantitative analysis of region of interesting (ROI) in the brain area indicated probe **12d** sufficiently penetrate the BBB and displayed considerable differences between Tg and WT at later time points. The fluorescence signal discrepancies between Tg and WT [F(Tg)/F(WT) ranging from 1.5 to 3.4] of **12d** were significantly higher than that DANIR 3b [F(Tg)/F(WT) ranging from 1.0 to 2.1] and DANIR 3c [F(Tg)/F(WT) ranging from 1.0 to 1.5] under the same dose and imaging parameters (Figure 4).

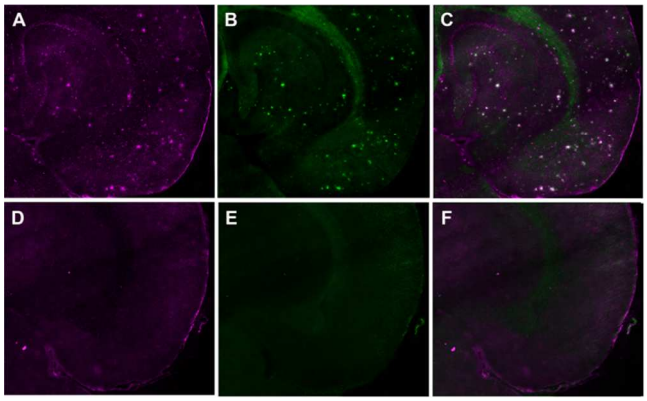

Figure 5. *Ex vivo* histopathological staining results of brain slices (cortex and hippocampus region) from a Tg mouse (C57BL6, APPsw/PSEN1, 19-month old, male) (A, Texas Red channel, 4X) and an age-matched WT mouse (C57BL6, 19-month old, male) (D, Texas Red channel, 4X) after dosing with **12d**. The homologous staining results were confirmed by ThS (B, E, GFP channel,). The merged images were shown in C and F, respectively.

Furthermore, after NIR imaging, subsequent *ex vivo* experiment was performed on Tg and WT mice to confirm the binding of **12d** to Aβ deposits. Fluorescence microscopy observation of the frozen brain sections in Figure 5 indicate that high signal-to-noise fluorescence spots were turned-on and mostly concentrated in the cortex and hippocampus regions of Tg mouse, while no specific signal was found in WT mouse brain. The same sections were further stained by Thioflavin-S (ThS) in GFP channel, and the spots merged well with the Texas Red channel of **12d** (Figure 5C). These results demonstrated probe **12d** could label Aβ plaques *in vivo* and effectively distinguish Tg and WT mouse.

CONCLUSIONS

In conclusion, we designed; synthesized and evaluated a series of D-π-A based Aβ probes with PEG modified acceptor. From *in vitro* studies, the PEG modified acceptors displayed very weak impact on emission wavelength, quantum yield, fluorescence enhancement upon binding to Aβ aggregates and binding affinity. The length of π bridge is still to be the dominant factor in above properties. Besides, the introduction of PEG chains caused the lipophilicity change as well as increased the molecule weight and size, and eventually led to decreased brain uptakes. In addition, Probe **12d** held a good capacity of crossing the BBB and favorable clearance rate from mice brain with improved brain kinetics compared with previously reported probes. Hence, PEG modification of the D-π-A probes is a direct and convenient way to adjust and improve their biological properties without changing much on optical properties. We believe that by carefully balancing the length of conjugated π system and PEG chains, we can obtain new NIR probes with better Aβ detection capability.

ASSOCIATED CONTENT

Supporting Information

The Supporting Information is available free of charge on the ACS Publications website.
Details of synthesis, additional figures, tables, NMR and MS spectra (PDF).

AUTHOR INFORMATION

Corresponding Author

*Phone/Fax: +86-10-58808891. E-mail: cmc@bnu.edu.cn.

Notes

The authors declare no competing financial interest.

ACKNOWLEDGMENT

This work was funded by the National Natural Science Foundation of China (No. 21571022), and the National Science and Technology Major Projects for Major New Drugs Innovation and Development (No. 2014ZX09507007-002).

REFERENCES

(1) Brookmeyer, R.; Johnson, E.; Ziegler-Graham, K.; Arrighi, H. M. *Alzheimer's Dementia* **2007**, *3*, 186-191.
(2) Hardy, J.; Higgins, G. *Science* **1992**, *256*, 184-185.
(3) Hardy, J.; Selkoe, D. J. *Science* **2002**, *297*, 353-356.
(4) Hardy, J. *J. Alzheimer's Dis.* **2006**, *9*, 151-153.
(5) J Soscia, S.; E Kirby, J.; Washicosky, K.; Tucker, S.; Ingelsson, M.; Hyman, B.; Burton, M.; Goldstein, L.; Duong, S.; E Tanzi, R.; Moir, R. *Plos One*, 2010; Vol. 5, p e9505.
(6) Kumar, D. K. V.; Choi, S. H.; Washicosky, K. J.; Eimer, W. A.; Tucker, S.; Ghofrani, J.; Lefkowitz, A.; McColl, G.; Goldstein, L. E.; Tanzi, R. E.; Moir, R. D. *Sci. Transl. Med.* **2016**, *8*, 340ra372-340ra372.
(7) Ono, M.; Saji, H. *Int. J. Mol. Imaging* **2011**, *2011*, 543267.
(8) Rowe, C. C.; Villemagne, V. L. *J Nucl Med* **2011**, *52*, 1733-1740.
(9) Staderini, M.; Martin, M. A.; Bolognesi, M. L.; Menendez, J. C. *Chem. Soc. Rev.* **2015**, *44*, 1807-1819.
(10) Weissleder, R.; Pittet, M. J. *Nature* **2008**, *452*, 580-589.
(11) Gibson, E. A.; Masihzadeh, O.; Lei, T. C.; Ammar, D. A.; Kahook, M. Y. *J. Ophthalmol.* **2011**, *2011*, 870879.
(12) Ntziachristos, V. *Annu. Rev. Biomed. Eng.* **2006**, *8*, 1-33.
(13) Ntziachristos, V. *Nat. Methods* **2010**, *7*, 603.
(14) Stuker, F.; Ripoll, J.; Rudin, M. *Pharmaceutics* **2011**, *3*, 229-274.
(15) Hintersteiner, M.; Enz, A.; Frey, P.; Jaton, A.-L.; Kinzy, W.; Kneuer, R.; Neumann, U.; Rudin, M.; Staufenbiel, M.; Stoeckli, M. *Nat. Biotechnol.* **2005**, *23*, 577-583.
(16) Li, Y.; Xu, D.; Ho, S.-L.; Li, H. W.; Yang, R.; Wong, M. S. *Biomaterials* **2016**, *94*, 84-92.
(17) Nesterov, E. E.; Skoch, J.; Hyman, B. T.; Klunk, W. E.; Bacskai, B. J.; Swager, T. M. *Angew. Chem. Int. Ed.* **2005**, *44*, 5452-5456.
(18) Ran, C.; Xu, X.; Raymond, S. B.; Ferrara, B. J.; Neal, K.; Bacskai, B. J.; Medarova, Z.; Moore, A. *J. Am. Chem. Soc.* **2009**, *131*, 15257-15261.
(19) Zhang, X.; Tian, Y.; Li, Z.; Tian, X.; Sun, H.; Liu, H.; Moore, A.; Ran, C. *J. Am. Chem. Soc.* **2013**, *135*, 16397-16409.
(20) Zhang, X.; Tian, Y.; Zhang, C.; Tian, X.; Ross, A. W.; Moir, R. D.; Sun, H.; Tanzi, R. E.; Moore, A.; Ran, C. *P. Natl. Acad. Sci. USA* **2015**, *112*, 9734-9739.
(21) Watanabe, H.; Ono, M.; Saji, H. *Chem. Comm.* **2015**, *51*, 17124-17127.

(22) Zhu, B. Y.; Cheng, Y.; Li, G. B.; Yang, S. Y.; Zhang, Z. R. *Bioorg. Med. Chem.*. **2016**, *24*, 827-834.
(23) Yang, H. Y.; Zhang, J. J.; Zang, Y.; Zhang, H. Y.; Li, J.; Chen, G. R.; He, X. P. *Dyes Pigm.* **2017**, *136*, 224-228.
(24) Zhu, J. Y.; Zhou, L. Y.; Li, Y. K.; Chen, S. B.; Yan, J. W.; Zhang, L. *Anal. Chim. Acta.* **2017**, *961*, 112-118.
(25) Ren, W.; Xu, M.; Liang, S. H.; Xiang, H.; Tang, L.; Zhang, M.; Ding, D.; Li, X.; Zhang, H.; Hu, Y. *Biosens. Bioelectron.* **2016**, *75*, 136-141.
(26) Fu, H.; Cui, M.; Tu, P.; Pan, Z.; Liu, B. *Chem. Comm.* **2014**, *50*, 11875-11878.
(27) Zhou, K. X.; Fu, H. L.; Feng, L.; Cui, M. C.; Dai, J. P.; Liu, B. L. *Chem. Comm.* **2015**, *51*, 11665-11668.
(28) Cui, M.; Ono, M.; Watanabe, H.; Kimura, H.; Liu, B.; Saji, H. *J. Am. Chem. Soc.***2014**, *136*, 3388-3394.
(29) Fu, H. L.; Cui, M. C.; Zhao, L.; Tu, P. Y.; Zhou, K. X.; Dai, J. P.; Liu, B. L. *J. Med. Chem.* **2015**, *58*, 6972-6983.
(30) Fu, H. L.; Tu, P. Y.; Zhao, L.; Dai, J. P.; Liu, B. L.; Cui, M. C. *Ana.l Chem.* **2016**, *88*, 1944-1950.
(31) Zhou, K.; Bai, H.; Feng, L.; Dai, J.; Cui, M. *Anal. Chem.* **2017**, *89*, 9432-9437.
(32) Harris, J. M.; Chess, R. B. *Nat. Rev. Drug Discovery* **2003**, *2*, 214.
(33) Zhang, W.; Oya, S.; Kung, M.-P.; Hou, C.; Maier, D. L.; Kung, H. F. *Nucl. Med. Biol.* **2005**, *32*, 799-809.
(34) Stephenson, K. A.; Chandra, R.; Zhuang, Z.-P.; Hou, C.; Oya, S.; Kung, M.-P.; Kung, H. F. *Bioconjugate Chem.* **2007**, *18*, 238-246.
(35) Li, Z.; Cui, M.; Dai, J.; Wang, X.; Yu, P.; Yang, Y.; Jia, J.; Fu, H.; Ono, M.; Jia, H. *J. Med. Chem.*. **2013**, *56*, 471-482.
(36) de Silva, A. P.; Gunaratne, H. Q. N.; Gunnlaugsson, T.; Huxley, A. J. M.; McCoy, C. P.; Rademacher, J. T.; Rice, T. E. *Chem. Rev.* **1997**, *97*, 1515-1566.
(37) Peccati, F.; Wisniewska, M.; Solans-Monfort, X.; Sodupe, M. *Phys. Chem. Chem. Phys.* **2016**, *18*, 11634-11643.
(38) Yao, L.; Zhang, S.; Wang, R.; Li, W.; Shen, F.; Yang, B.; Ma, Y. *Angew. Chem. Int .Ed. Engl.***2014**, *53*, 2119-2123.
(39) Mathis, C. A.; Wang, Y.; Holt, D. P.; Huang, G.-F.; Debnath, M. L.; Klunk, W. E. *J. Med. Chem.* **2003**, *46*, 2740-2754.
(40) Waterhouse, R. N. *Mol. Imaging Biol.* **2003**, *5*, 376-389.

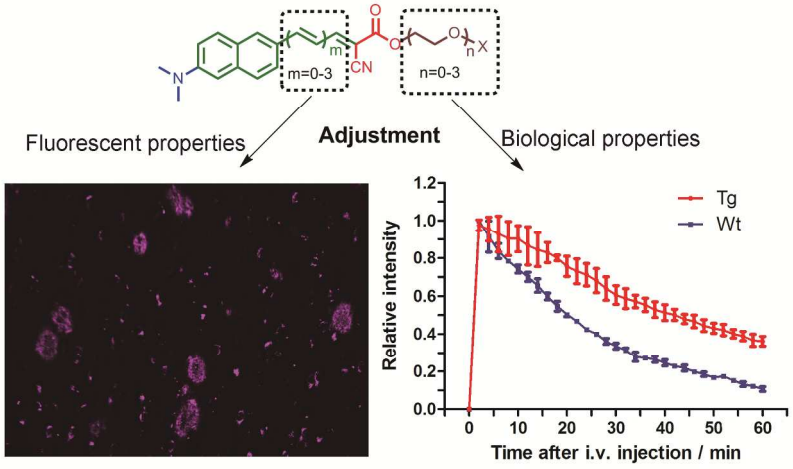

Insert Table of Contents artwork here

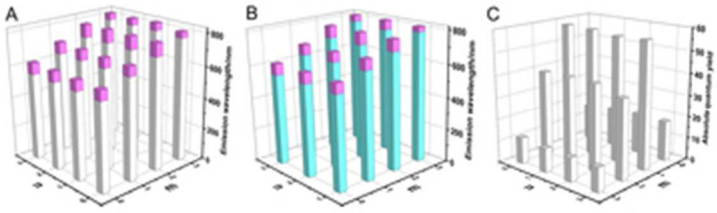

Figure 1. Fluorescent properties associated with the length of conjugated double bond and PEG chain. (A) Maximum emis-sion of methoxyl-ended probes (8a-d to 10a-d) measured in CH2Cl2 (white) and PBS (magenta). (B) Maximum emission of hydroxyl-ended probes (11a-d to 13a-d) measured in CH2Cl2 (cyan) and PBS (magenta). (C) Absolute quantum yield of methoxyl-ended probes (7a-d to 10a-d) determined in CH2Cl2.

30x9mm (300 x 300 DPI)

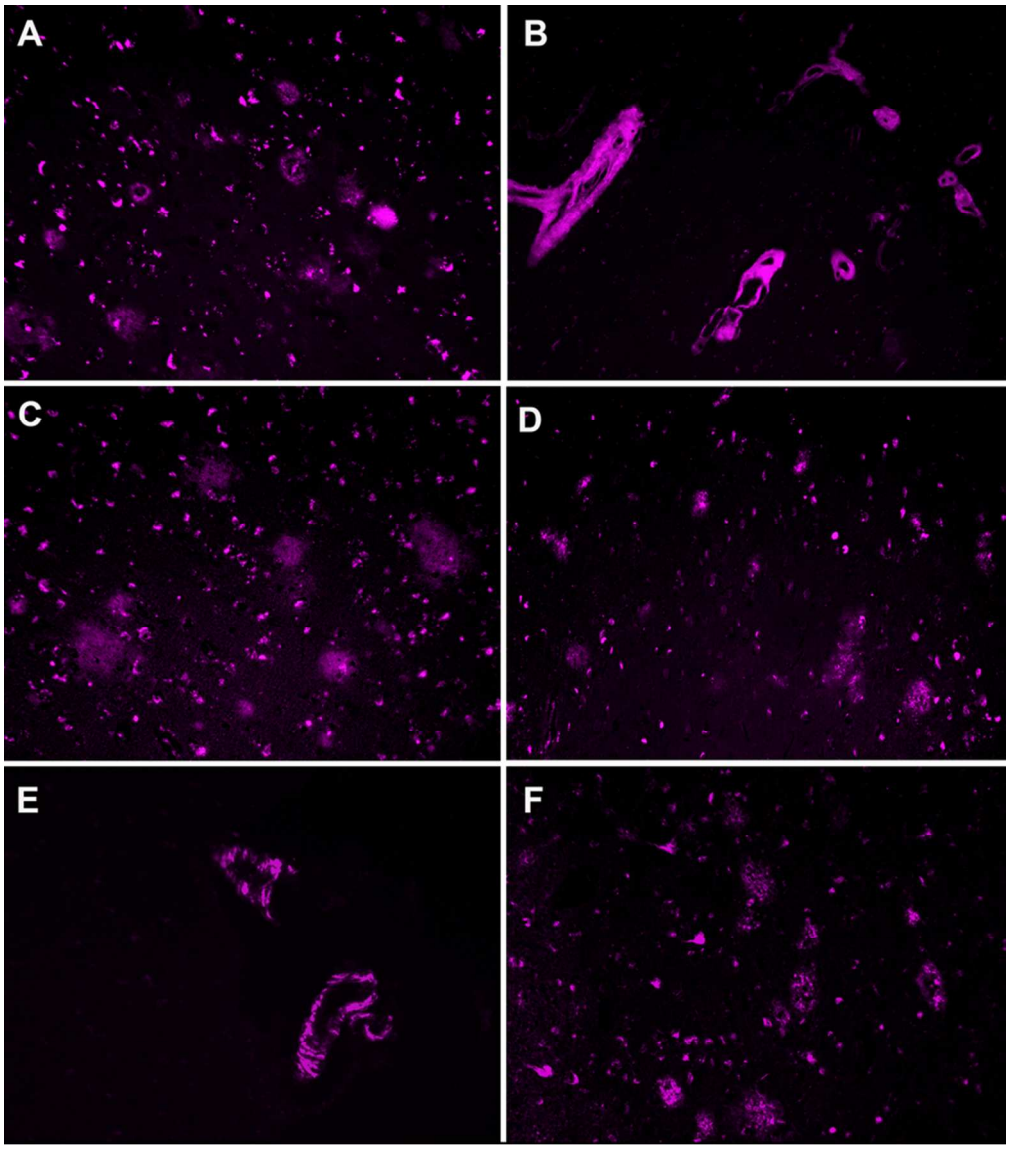

Figure 2. In vitro histopathological fluorescence staining of probe 12d on brain slices from patients of AD and CAA. (A) AD tissue, 64-year old, female, temporal lobe, 20X; (B) CAA tissue, 68-year old, female, temporal lobe, 10X; (C) AD tissue, 71-year old, female, temporal lobe, 20X; (D) AD tissue, 85-year old, male, temporal lobe, 20X; (E) CAA tissue, 76-year old, male, temporal lobe, 20X; (F) AD tissue, 91-year old, male, temporal lobe, 20X.

75x86mm (300 x 300 DPI)

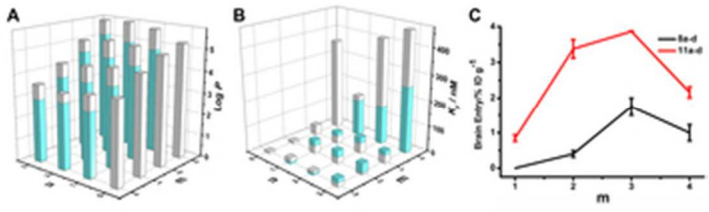

Figure 3. (A) The clogP value of the NIRF probes 7a - 10d (methoxyl-ended probes) (white), 11a - 13d (hydroxyl-ended probes) (cyan), calculated by the online ALOGPS 2.1 program. (B) Kd value for 7a - 10d (white), 11a - 13d (cyan). (C) Initial brain uptake of the 8a - 8d (black curve) and 11a -11d (red curve) after i.v. injection at 2 min.

29x8mm (300 x 300 DPI)

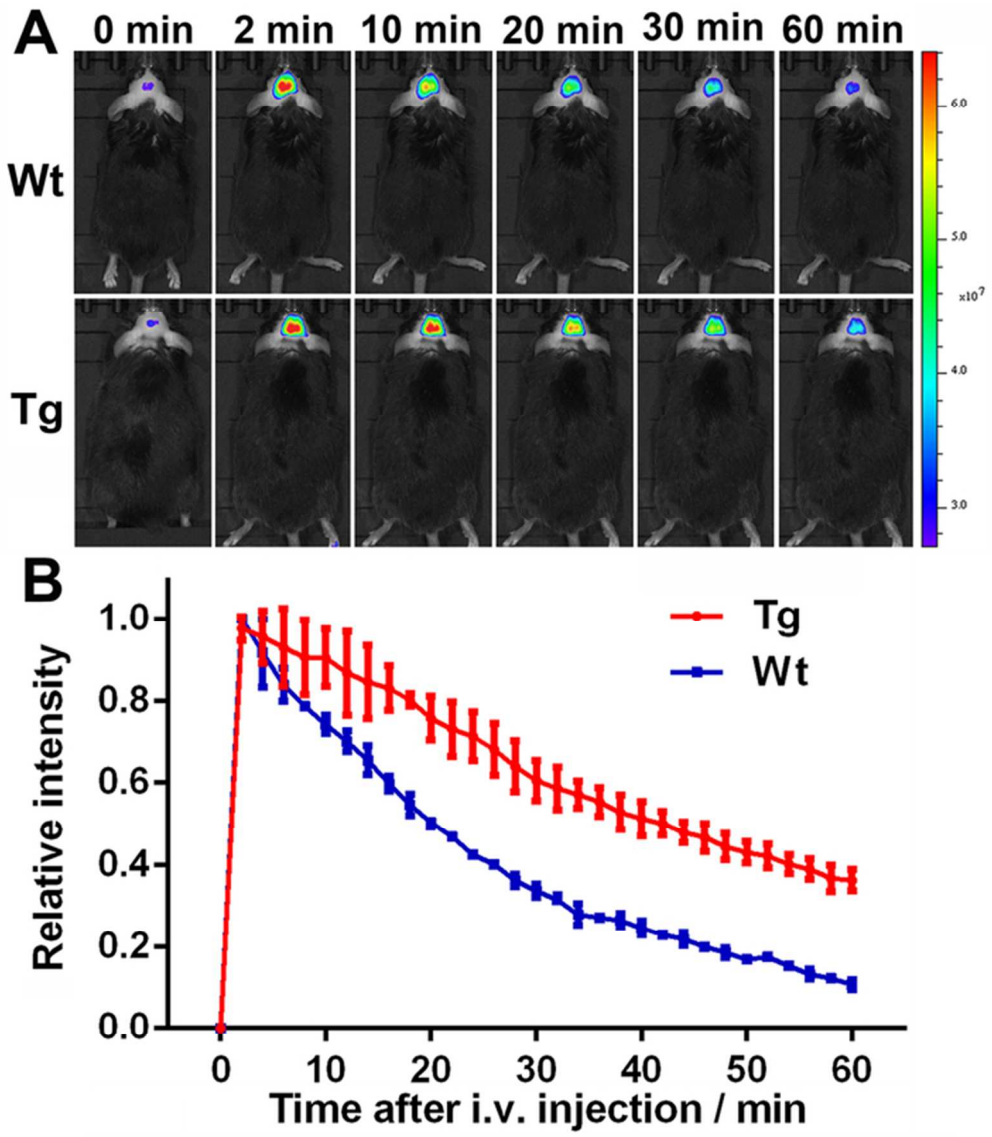

Figure 4. (A) In vivo NIR brain images from Tg and WT control mouse on representative time points before and after i.v. injection of probe 12d. (B) Quantitative analysis of the relative fluorescence signals to show the brain kinetic curves of probe 12d at selected time points.

60x67mm (300 x 300 DPI)

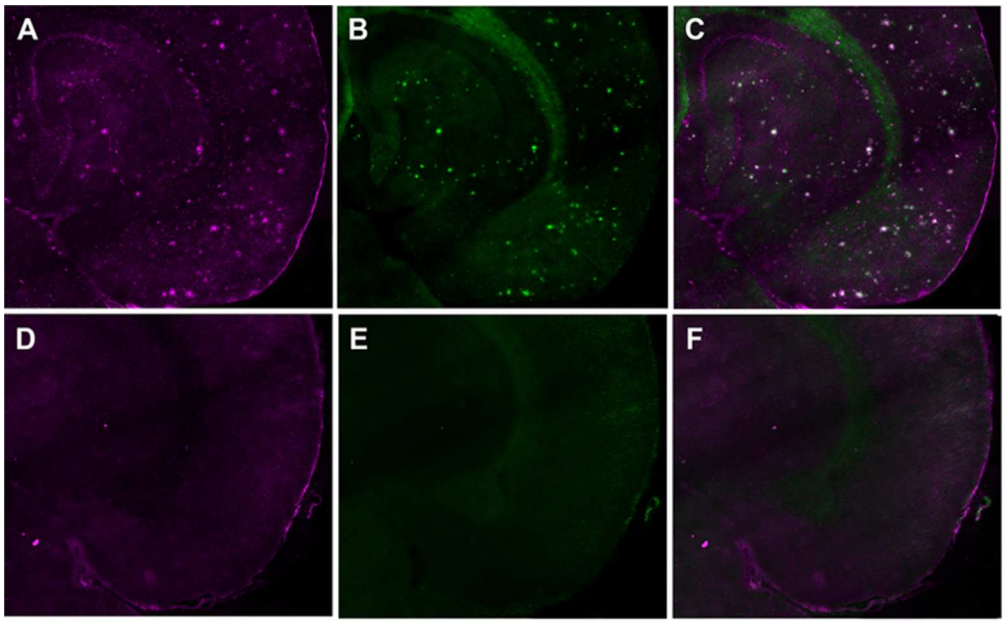

Figure 5. Ex vivo histopathological staining results of brain slices (cortex and hippocampus region) from a Tg mouse (C57BL6, APPsw/PSEN1, 19-month old, male) (A, Texas Red channel, 4X) and an age-matched WT mouse (C57BL6, 19-month old, male) (D, Texas Red channel, 4X) after dosing with 12d. The homologous staining results were confirmed by ThS (B, E, GFP channel,). The merged images were shown in C and F, respectively.

62x38mm (300 x 300 DPI)

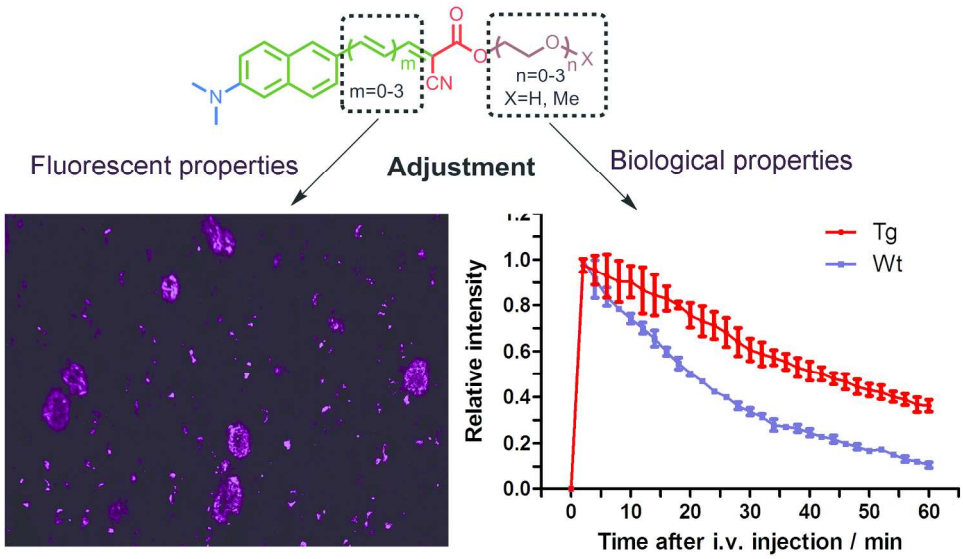

182x110mm (300 x 300 DPI)